Novel ZnO nanostructures over gold and silver nanoparticle assemblies

Vivek Pachauri [1], Chandramouli Subramaniam, T. Pradeep *

DST Unit on Nanoscience, Department of Chemistry and Sophisticated Analytical Instrument Facility, Indian Institute of Technology Madras, Chennai 600036, India

Abstract

We report the growth of well-oriented nest (reticulum)-like and lotus flower-like submicron structures of ZnO, over gold and silver nanoparticle assemblies, respectively. The structures were grown by a convenient chemical bath deposition method in a nutrient solution made of zinc nitrate $(Zn(NO_3)_2 \cdot 6H_2O)$ and methyl amine (CH_3NH_2) at low temperature. SEM, XRD, Raman, UV–Vis and fluorescence spectra were used to study the morphology, crystallinity and phase purity of the structures. The ZnO submicron structures were found to be in the hexagonal wurtzite phase.
© 2006 Elsevier B.V. All rights reserved.

1. Introduction

In recent years, synthesis of inorganic materials with specific size and morphology has attracted significant attention due to their possible use in different fields [1–3]. There are reports of synthesizing many interesting nanostructures of ZnO including funnels, straw bundles, feathers, nanorods/nanopillars, nanotubes, nanorings, disks, dendrites, tetrapods, multipods and many other low dimensional structural forms [4–9]. Procedures are being developed to synthesize materials with controlled morphologies and unique properties exploring unusual methods of self-assembly.

ZnO is a valuable electronic and photonic material [10,11] because of its wide direct bandgap energy of 3.67 eV and large exciton binding energy of 60 meV [12,13]. Nanocrystalline ZnO also possesses excellent chemical and thermal stability. Because of its unique properties, ZnO is employed to make devices, applicable in different fields of science and daily life. Nanocrystalline ZnO is widely used for making acoustic wave filters [14], photonic crystals [15], UV photo detectors, field effect transistors, intramolecular p–n junction diodes, schottky diodes, photo-diodes [16], light-

emitting diodes [17], optical modulator wave guides [18] and gas-sensors [19]. This is an exceptionally important material having applications in pigments, rubber additives, varistors and optical devices and thus interesting for both research and practical studies. ZnO is also known to have anti-bacterial properties and along with its arsenic scavenging ability finds use in water treatment and purification.

Since the first report on UV lasing, substantial effort has been devoted towards the development of different preparative methods such as arc discharge, laser vaporization, pyrolysis, electro- deposition and chemical vapour deposition (CVD) to grow these nanostructures. Most of these processes are restricted to rigid experimental conditions and require costly equipment. Instead, soft chemical route facilitates the approach to scale up the structures with relatively low cost, and at low temperatures. The approach of environmentally safe and benign chemical bath deposition method allows further reduction of the growth temperature to 70–80 °C, leading to efficient and low cost fabrication of novel ZnO structures.

2. Experimental

$HAuCl_4 \cdot 6H_2O$ was purchased from CDH and zinc nitrate hexahydrate was from Merck. All the other chemicals used in the synthesis were from the local sources. The chemicals used in the experiment were of the best purity

---

* Corresponding author.
  E-mail address: pradeep@iitm.ac.in (T. Pradeep).
[1] Summer research fellow of Jawaharlal Nehru Center for Advanced Scientific Research from Dr. B. R. Ambedkar University Agra, India.

available. One-side conducting glass plates having an electrically conducting surface of indium tin oxide (ITO) with a resistivity of 70 Ω cm were used throughout this work.

The glass plates were cleaned in a mild detergent solution with the help of a sonicator to remove any greasy contamination. After sonication in 10% HCl solution to remove salt impurities, glass plates were subjected to repeated washings with methanol to remove any physisorbed impurities. These properly cleaned glass slides were then annealed at 450 °C for 7 h. The slides were then subjected to silanization using 30 mM 3-aminopropyl triethoxy silane (3-APS) solution in toluene for 45 min at room temperature. Removing the slides from APS solution, washing and sonication was performed repeatedly in methanol to remove any physisorbed APS. Slides were subsequently annealed for 4 h at 110 °C. Thus, the slides having a silane layer were prepared which have been used as wafers for developing the assemblies of gold and silver nanoparticles. Silanised slides were treated with gold nanoparticles solution separately for 30 min at room temperature and a gold nanoparticle assembly was prepared. The gold colloid ($\sim$15 nm dia.) was prepared by the citrate

reduction method [20,21]. Slides were also treated with silver nanoparticle (30–60 nm dia, citrate reduction) solution for 30 min. at room temperature. Schematic of the process is illustrated in Scheme 1. UV–Vis absorption spectra were measured for these assembled surfaces (Fig. 1) using a Perkin–Elmer Lambda 25 UV–Vis absorption spectrophotometer. The multiple peaks in the absorption spectrum arise due to the interplasmon coupling between the nanoparticles in the assembly [22]. The slides thus obtained were then subjected to further silanization to coat an additional layer of silane. To achieve this, slides were kept in 3-APS solution for 45 min at room temperature. A red shift of $\sim$5 nm in the UV–VIS spectrum was observed due to the chemisorption of APS.

The processed slides were dipped (kept in an even level on the work bench) into the reaction mixture (ZnO precursor) taken in a beaker. Reaction mixture was made with 0.045 M zinc nitrate and 0.045 M methylamine in distilled water. The beaker was placed in a hot air oven at 70 °C for 1 h and then temperature was increased up to 80 °C. The beaker was taken out of the oven after 9 h and slides were removed from the reaction mixture, washed properly
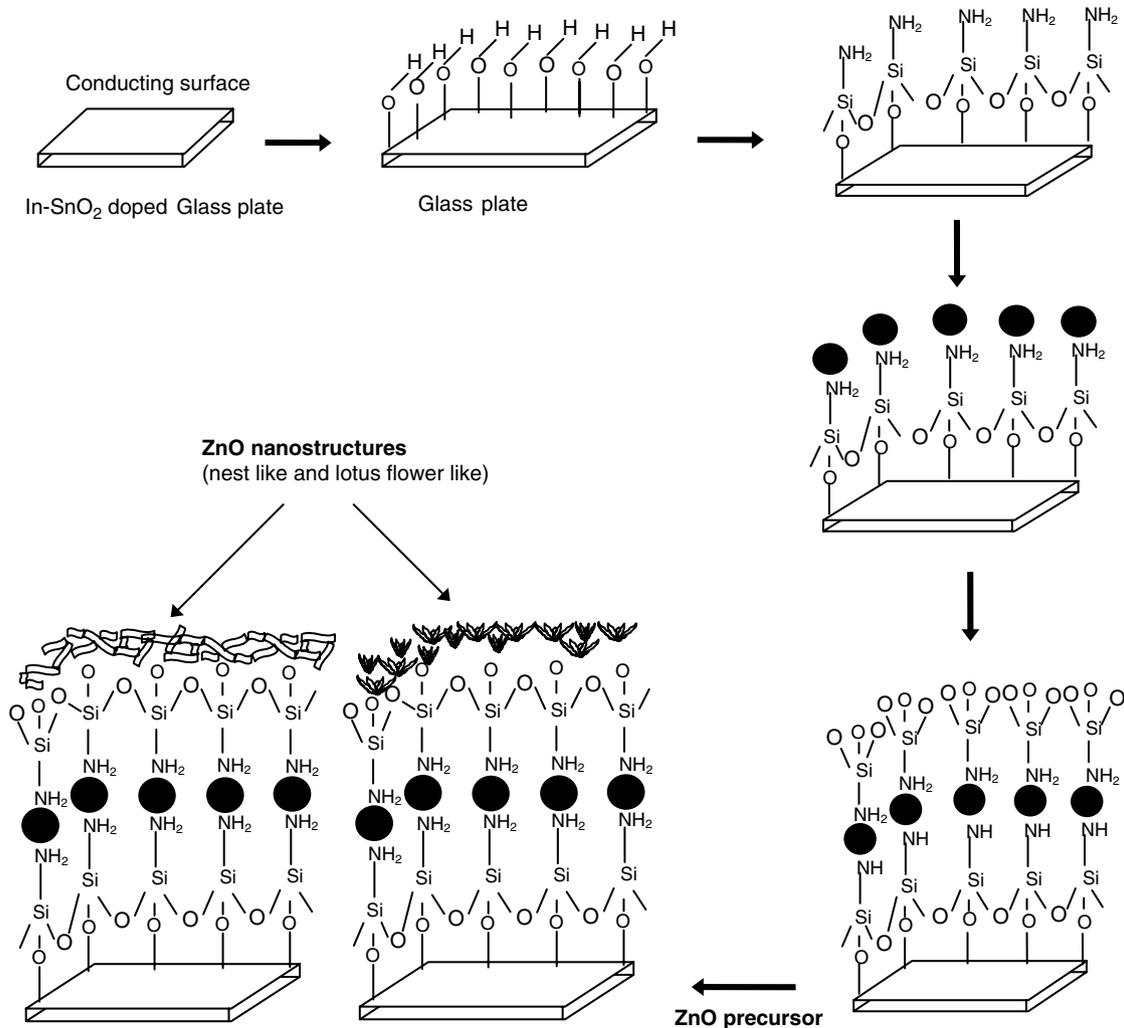
Scheme 1. Sequence of steps involved in the preparation of nanostructures.
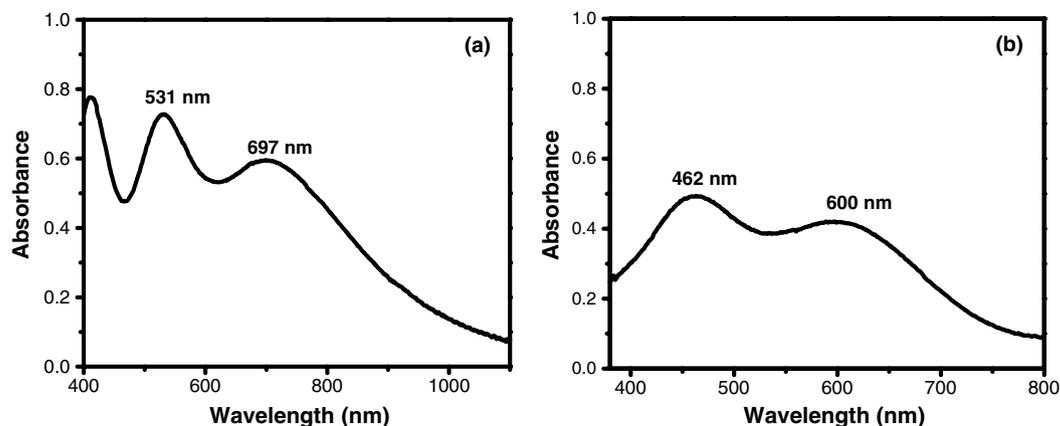
Fig. 1. UV–Vis absorption spectra of gold (a) and silver (b) nanoparticle assemblies. The peaks at 531 nm and 462 nm are due to gold and silver nanoparticles, respectively. The peaks in the red region are due to inter-plasmon coupling in the nanoparticle film.

with distilled water and put into the desiccator for drying. It could be seen clearly that an ultra thin layer of ZnO was developed over the whole conducting glass surface. Schematic of the events is depicted in Scheme 1.

To know the exact morphology of the ZnO film grown over gold and silver nanoparticle assembly, SEM measure-ments were done using JEOL JSM 5600 LV Scanning Elec-tron Microscope. X-ray diffraction analysis was carried out using a Shimadzu XD D10 Diffractometer with Cu Kα radiation ($\lambda = 1.54$ Å). Vibrational properties and phase purity were investigated by the Raman spectra, measured using a WiTec confocal Raman Spectrometer. The excita-
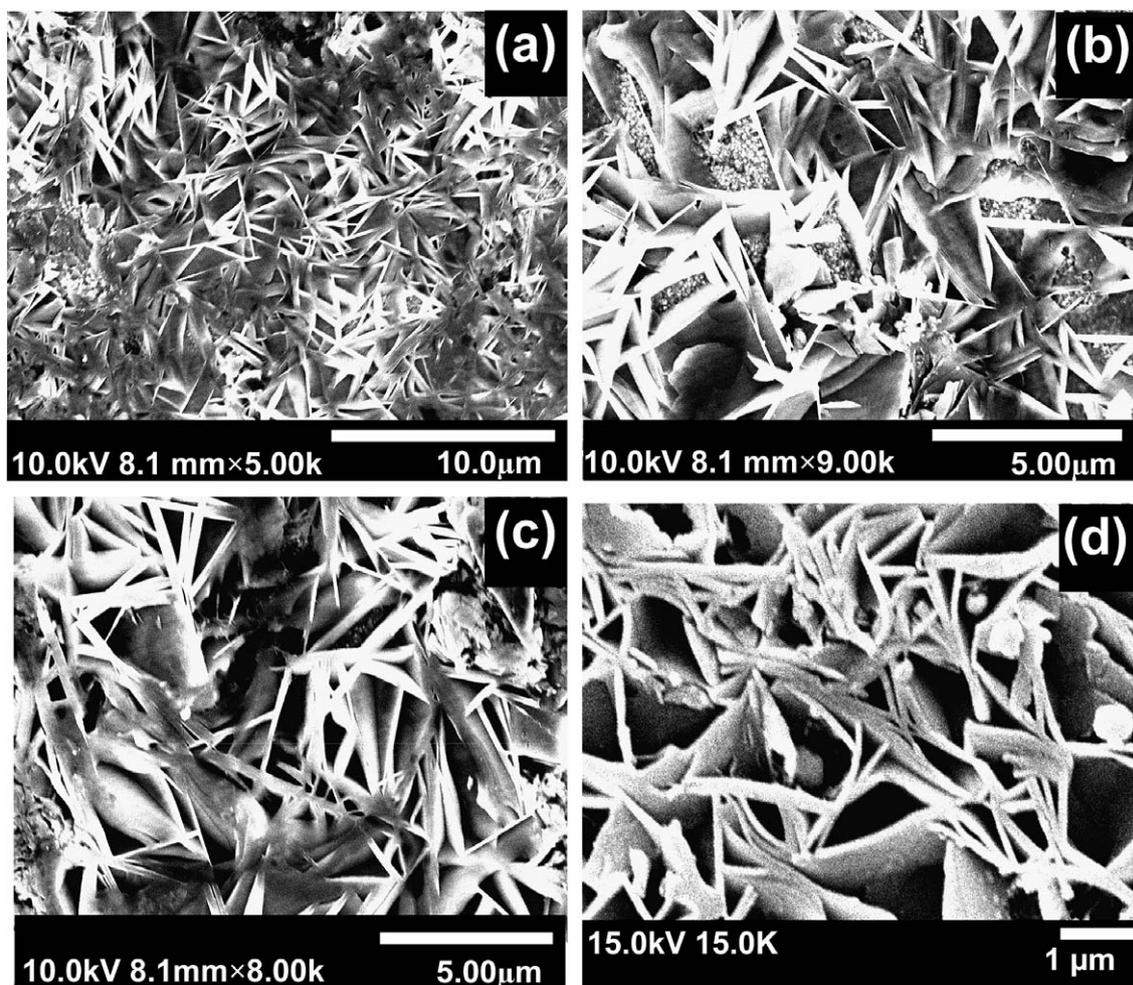
Fig. 2. SEM images of nest-like micron structures ZnO grown over gold nanoparticle assembly. Image showing dense network of structures (a), (b), (c) and (d) are at magnifications 5000×, 9000×, 8000× and 15 000×, respectively.

tion source used was an Ar ion laser of 514.5 nm wavelength. The Raman signal was collected in a back-scattering geometry after passing through a super-notch filter. A peltier cooled CCD was used as the detector and the signal was dispersed using an 1800 grooves/mm grating. A room temperature fluorescence spectrum was measured using a Jobin–Vyon fluorolog fluorescence spectrometer.

3. Result and discussion

Fig. 2 shows a set of SEM images of the as grown films prepared over Au nanoparticle assemblies at different magnifications. Image a shows highly dispersed nest-like (reticulum like) structures grown over the entire surface. Images b–d are of higher magnifications. Many lamellar structures aligned perpendicular to the surface were seen in the images. Due to random link-up between the ends of these lamellar nanostructures many cavities are formed. In the last image d, a closer view of the structures is seen. The lamellae intersect each other randomly and make sharp angles at the point of merging. These lamellar structures running into each other give an appearance of a dense network of a reticulum. The cross-linked and equally thickened lamellae finally create nano/micron sized cavities of different shapes and sizes. The cavities range from 0.5 μm to 2.5 μm in diameter.

Fig. 3 shows a set of SEM images of the film grown over the silver nanoparticle assembly. Here, the sample was sculptured in the form of well-oriented micron sized structures, appearing as lotus flowers. These unique structures were found to be well distributed and uniform on the surface, indicating that the underlying self-assembled layer of silver nanoparticle plays a vital role in the formation of these structures.

The structures observed in Fig. 2a–d, obtained with gold self-assembled surfaces, are in stark contrast to the Fig. 3a–f, obtained with silver self-assembled surfaces. This clearly shows that the growth of ZnO follows a template-based approach, with the geometry and assembly of the underlying nanoparticle network providing the orientation for the directed growth of the ZnO structures. The highly ordered and oriented growth of these structures could be due to the self-assembly of silver nanoparticles. Images 3a–d were taken at different magnifications. Fig. 3b and c show the growth of the sample in the form of well-oriented flower-like structures which are dispersed well over the surface. The flowers looked like broad and smooth conical outgrowths pointed at their distal ends. The conical outgrowths are symmetrical and extend radially from the centre. Image d taken at higher magnification gives a closer look of the micron sized flower-like structures ranging
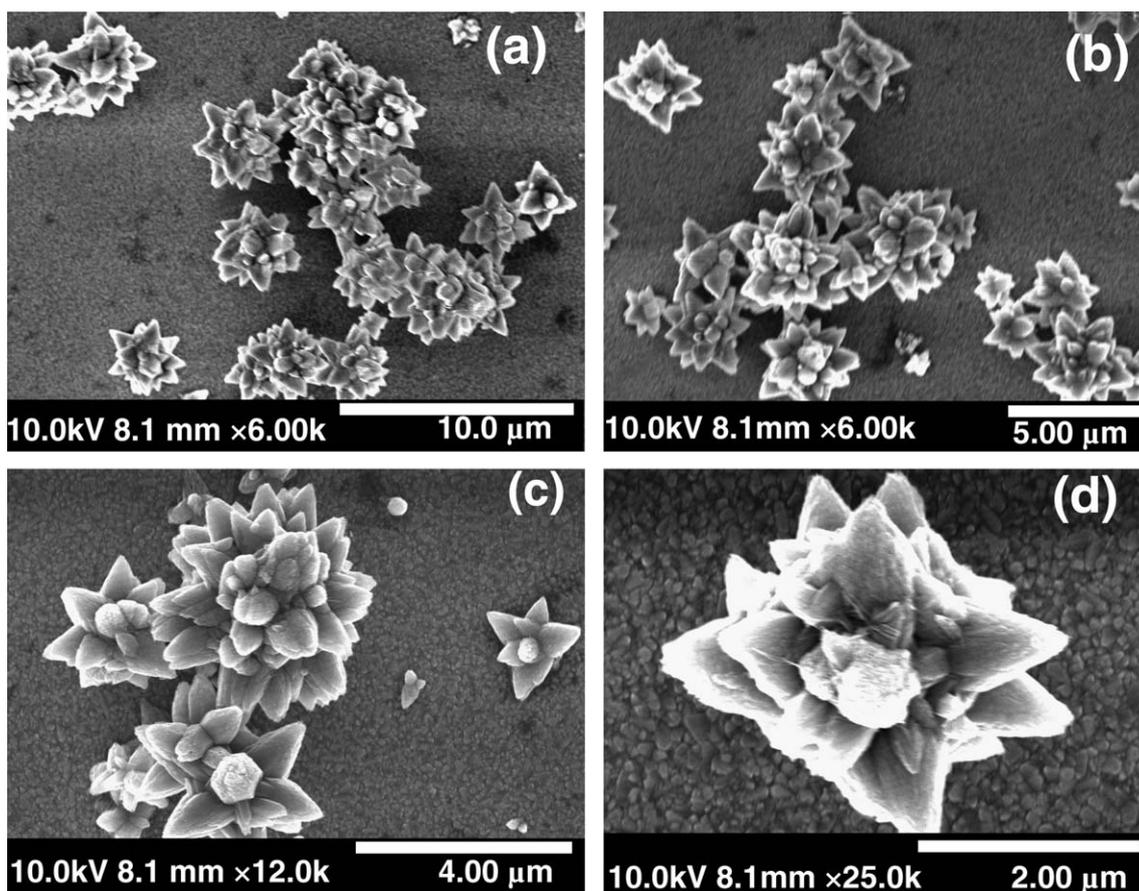
Fig. 3. SEM images of the flower-like ZnO micron structures grown over a silver nanoparticle assembly. Image (a), (b) and (c) show the lotus flower-like micron structures grown over the surface. The higher magnification image (d) shows well-oriented flower shaped structures.

from 1.5 μm to 4 μm. The petal like structures make several whirls one over the other to look like a lotus.

Fig. 4a, b show the XRD patterns of the products grown over gold and silver nanoparticle assemblies, respectively. Clearly, all the peaks in both the patterns are consistent with the values of the standard (JCPDS 36-1451) and can be indexed to pure ZnO with a hexagonal wurtzite structure. Peaks marked with an asterisk are due to the glass plate. No peaks due to impurities were detected. Peaks at $2\theta = 31.8°$, $34.5°$ and $36.5°$ are attributed to ZnO (100), (002) and (101) planes, respectively. The larger intensity of the (100) peak indicates that the product over the gold nanoparticle assembly is grown preferentially along the *c*-axis. This is in agreement with the aligned growth of the structures perpendicular to the surface as seen in SEM images. From the XRD pattern and SEM images, it is clear that these lamellar structures of ZnO are grown along the [0001] direction and exhibit single crystalline wurtzite phase. A relatively weak (002) in the case of the Ag nanoparticle film indicate that the growth is not preferred along the *c*-axis. All the other peaks are assigned to hexagonal single crystalline wurtzite phase of ZnO.

Raman measurements were performed to investigate the vibrational properties and phase purity of the ZnO structures. ZnO crystallizes in the hexagonal wurtzite form and belongs to C_{6v} space group. According to the symme-

try selection rules, there are eight phonon modes for the wurtzite phase belonging to $2E_2$, $2E_1$, $2A_1$ and $2B_2$ symmetries. Of these, two symmetry modes ($2B_2$) are not Raman active. Additionally, A_1 and E_1 are also IR active and split into longitudinal (LO) and transverse (TO) optical components exhibiting different frequencies. Non-polar phonon modes with symmetry E_2 have two frequencies; E_2 (high) and E_2 (low) associated with oxygen and Zn sublattices, respectively.

Fig. 4 includes Raman spectra of the products grown. The spectrum of the nest-like nanostructures is shown in Fig. 4c. Peaks were observed at 327 cm^{-1}, 333 cm^{-1} and 573 cm^{-1} corresponding to IInd-E_2, E_2 and A_1 (LO) and E_1 (LO) modes, respectively [23]. The peaks suggest the presence of the wurtzite phase. Peaks at 330 cm^{-1}, 436 cm^{-1} and 577 cm^{-1} are observed for the product grown over silver nanoparticle assembly corresponding to IInd E_2, E_2 and A_1-(LO) and E_1 (LO) modes, respectively (Fig. 4d). All phonon modes reported in the Raman spectra from these nanostructures were in good agreement when compared with the theoretical calculations of Fonoberov and Balandin for bulk ZnO [24,25].

Raman spectra for both the products grown (Fig. 4c, d) show suppressed peaks at 573 cm^{-1} and 577 cm^{-1}, respectively, which were assigned to be the E_1-LO mode. It is widely believed that the appearance of the E_1-LO mode
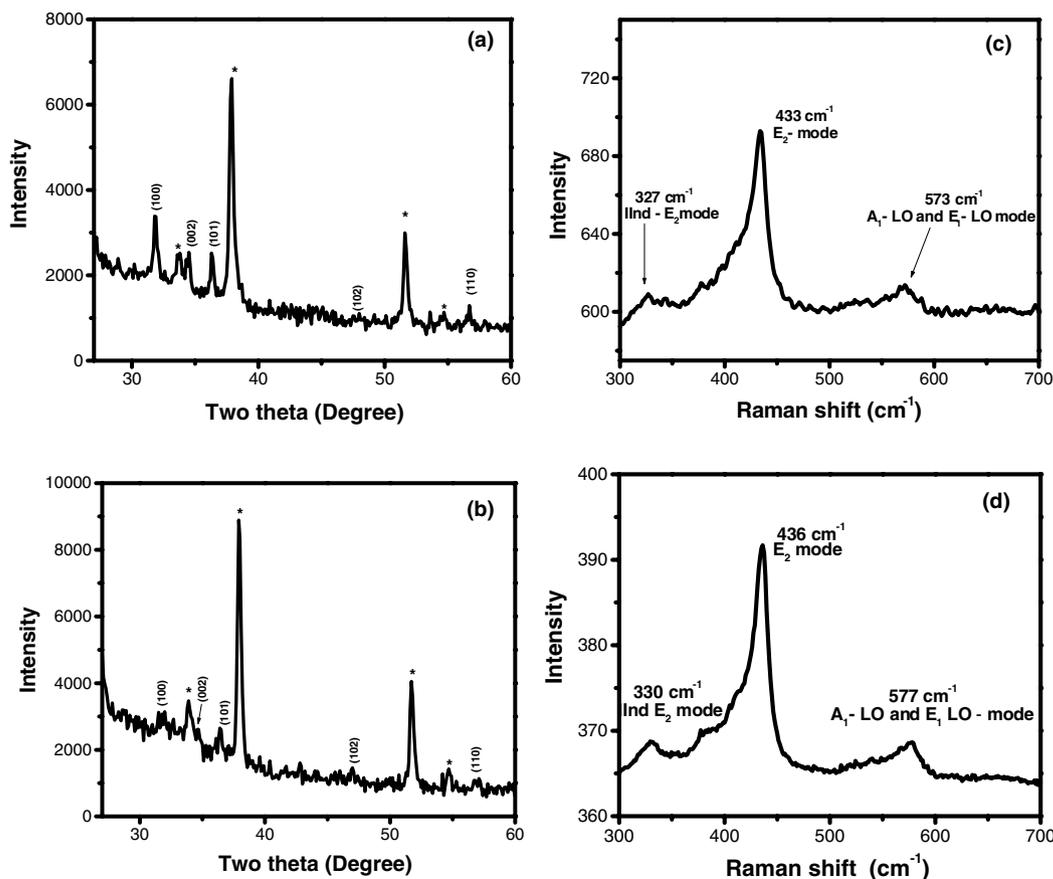
Fig. 4. XRD patterns for ZnO films grown over gold (a) and silver (b) nanoparticle assemblies. The diffraction pattern shown in the inset is due to the substrate (glass plate). Raman scattering spectra are for the ZnO film grown over gold (c) and for silver (d) nanoparticle assemblies.
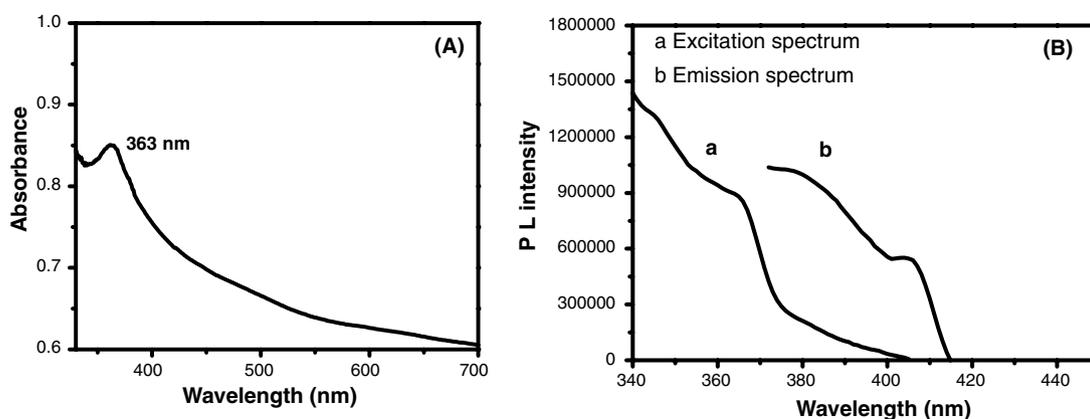
Fig. 5. The UV–Vis absorption spectrum (A) and fluorescence spectrum (B) for the ZnO film grown over silver nanoparticle assembly. (a) Excitation spectrum and (b) emission spectrum. Excitation peak is at 365 nm, and the emission peak is at 406 nm.

in the Raman scattering is because of impurities and structural defects (oxygen vacancies and zinc interstitials) of the products grown. Finally, the appearance of the sharp E_2 (high) mode corresponds to the characteristic wurtzite phase and suppressed E_1 peak suggests that the grown nanostructures are good in crystallinity. No contamination in the samples was found in EDAX analysis and therefore, structural defects are the sole reason for the appearance of the E_1-LO mode.

Fig. 5 shows the absorption and luminescence spectra of the product. A typical exciton absorption band at 363 nm was observed in the absorption spectrum (Fig. 5A) that is blue shifted with respect to the bulk absorption edge [26] (appearing at 400 nm at room temperature). A photoluminescence peak appearing at 406 nm in the emission spectrum (Fig. 5B) can be attributed to the electron–hole recombination. The excitation spectrum shown in Fig. 5B was measured for emission at 406 nm [27].

Gold and silver nanostructure assemblies provide heterogeneous nucleation sites for the growth. According to the classical theory of nucleation and growth, the homogenous nucleation of metal oxides has a higher activation energy barrier so that heterogeneous nucleation will be favored [28].

This chemical approach to synthesize different ZnO nanostructures is based on the use of different nanoparticle assemblies as structure directing agents. Such assemblies are believed to provide different orientation factor for the growth of ZnO nanostructures as per their geometry and assembling pattern. The other preparative parameters such as initial reactant concentrations and reaction time were kept same in the reactions and structure directing chemicals such as ligands or surfactants were used. The method also offers high synthetic flexibility and good controllability over the targeted product morphology.

4. Conclusion

Nest-like (reticulum like) structures and flower-like structures of ZnO were grown over gold and silver nanoparticles assemblies, respectively. UV–Vis spectra, SEM, XRD and

Raman were used for the characterization of these novel structures. The novel structures were found to exhibit a single crystalline hexagonal wurtzite phase. Interestingly, gold nanoparticle and silver nanoparticle assemblies were leading to different type of ZnO nanostructures in the very same reaction conditions. The method is advantageous as it is cheap, easily controlled and environmentally safe. Nest-like microstructures of ZnO are quite interesting because of their unique morphology. The sub-micron sized cavities can enhance the sensing properties of nanocrystalline ZnO leading to its use in more sophisticated and advanced devices. As ZnO possess anti-bacterial and arsenic scavenging properties, these structures can find application in fabricating some useful germicidal and prophylactic devices.

References

[1] X. Duan, Y. Huang, R. Agrawal, C.M. Lieber, Nature 421 (2003) 241.
[2] M.S. Fuhrer, J. Nygard, L. Shih, M. Forero, Y.G. Yoon, M.S.C. Mazzoni, H.J. Choi, Science 288 (2000) 494.
[3] Z.F. Ren, Z.P. Huang, J.W. Xu, J.H. Wang, P. Bush, M.P. Siegal, P.N. Provencio, Science 282 (1998) 1105.
[4] S.H. Yu, M. Antonietti, H.C. Olfen, Hartmann, Nano. Lett. 3 (2003) 379.
[5] R. Zhang, X.Y. Chen, M.S. Mo, Z.H. Wang, M. Zhang, X.Y. Liu, Y.T. Qian, J. Cryst. Growth 262 (2004) 449.
[6] H.M. Hu, Z.P. Liu, B.J. Yang, M.S. Mo, Q.W. Li, W.C. Yu, Y.T. Qian, J. Cryst. Growth 262 (2004) 375.
[7] X. Peng, Adv. Mat. 15 (2003) 459.
[8] M.H. Huang, S. Mao, H. Feick, H. Yan, Y. Wu, H. Kind, E. Weber, R. Russo, P. Yang, Science 292 (2001) 1897.
[9] Z.K. Tang, G.K.L. Wong, P. Yu, M. Kawasaki, A. Ohtomo, H. Koinuma, Y. Segava, Appl. Phys. Lett. 72 (1998) 3270.

[10] J.T. Hu, T.W. Odom, C.M. Lieber, Acc. Chem. Res. 32 (1999) 435.

[11] Z.W. Pan, Z.R. Dai, Z.L. Wang, Science 291 (2001) 1947.

[12] D. Andeen, L. Loeffler, N. Padture, F.F. Lange, J. Cryst. Growth 259 (2003) 103.

[13] Y. Chen, D.M. Bagnall, H. Ko, K. Park, K. Hiraga, Z. Zhu, T. Yao, J. App. Phys 84 (1998) 3912.

[14] N.W. Emanetoglu, C. Gorla, Y. Lu, Mat. Sci. Semicond. Process 2 (1999) 247.

[15] Y.D. Bagnall, T. Yao, Mater. Sci. Eng. B 75 (2000) 190.

[16] J.Y. Lee, Y.S. Choi, J.H. Kim, M.O. Park, S. Thin Solid Films 403 (2002) 533.

[17] N. Saito, H. Haneda, T. Sekiguchi, N. Ohashi, I. Sakaguchi, K. Koumoto, Adv. Mater. 14 (2002) 418.

[18] M.H. Koch, P.Y. Timbrell, R.N. Lamb, Semicond. Sci. Technol. 10 (1995) 1523.

[19] N. Goligo, S.A. Studenikin, M.J. Cocivera, Electrochem. Soc. 147 (2000) 1592.

[20] J. Turkevitch, P.C. Stevenson, J. Hillier, Discuss. Faraday Soc. (1951).

[21] J. Turkevitch, Gold Bull. 18 (1985) 86.

[22] C.P. Collier, R.J. Saykally, J.J. Shiang, S.E. Henrichs, J.R. Heath, Science 277 (1997) 1978.

[23] T.C. Damen, S.P.S. Porto, S.;B. Tell, Phys. Rev. 142 (1966) 570.

[24] K.A. Alim, V.A. Fonoberov, A.A. Balandin, Appl. Phys. Lett. 86 (2005) 053103.

[25] V.A. Fonoberov, A.A. Balandin, Phys. Cond. Mat. 17 (2005) 1085.

[26] W.Y. Liang, A.D. Yoffe, Phys. Rev. Lett. 20 (1968) 59.

[27] K. Vanheusden, C.H. Seager, W.L. Warren, D.R. Tallant, J.A. Voigt, Appl. Phys. Lett. 68 (1996) 403.

[28] J.W. Mullin, Crystallization, fourth edn., Butterworth-Heinemann, London, 2001.